Interdisciplinary Research in Medical Sciences Specialty
ISSN: 3062-4401
2026, Volume 6, Issue 1, Page No: 1-14

Available online at: www.galaxypub.co/page/journals

Galaxy Publication

A Scalable Automated Platform for Immune Tumor Organoids Enables Functional Evaluation of Chemo-Immunotherapy

Rafael Mendoza[1]*, Isabela Cruz[1], Carlos Lopez[2]

[1]Department of Tumor Organoids and Immunotherapy, Faculty of Medicine, National Autonomous University of Mexico, Mexico City, Mexico.
[2]Department of Chemo-Immunotherapy Drug Screening, Faculty of Medicine, Monterrey Institute of Technology, Monterrey, Mexico.

***E-mail** ✉ rafael.mendoza@unam.mx

Received: 15 September 2025; **Revised:** 05 January 2026; **Accepted:** 08 January 2026

ABSTRACT

Drug resistance frequently emerges in breast cancer during chemotherapy, and standalone immunotherapies often yield insufficient results. Therefore, the clinical advancement of combined chemo-immunotherapy strategies is critically needed. However, traditional two-dimensional cell cultures and animal models remain inadequate for reliably assessing the outcomes of such combined treatments. This study presents a straightforward automated multi-well system developed for producing tumor-associated macrophages (TAMs)-immunized breast cancer organoids encapsulated in alginate hydrogels. Using an automated robotic microinjection approach, alginate hydrogels were formed in situ, followed by the introduction of mixed suspensions containing breast cancer cells and TAMs to generate organoids. Breast cancer organoids incorporating TAMs displayed pronounced resistance to epirubicin, yet this effect was effectively reversed by the targeted immunotherapeutic agent PLX3397. Synergistic benefits were systematically examined through multiple schedules of co-administering PLX3397 alongside epirubicin. Complementary RNA sequencing and quantitative polymerase chain reaction analyses were performed to profile gene expression changes under co-treatment conditions, revealing three significantly altered genes—IL6, CD37, and GLS2—that participate in the tumor necrosis factor signaling pathway, PI3K-Akt signaling pathway, and epidermal growth factor receptor tyrosine kinase inhibitor resistance pathway. Overall, these results highlight the capacity of the automated multi-well platform to serve as a viable substitute for conventional bulk culture techniques in the evaluation of chemo-immunotherapy efficacy.

Keywords: Breast cancer, Chem-immunotherapy, Hydrogels, Immunized tumor organoids, Tumor associated macrophages

How to Cite This Article: Mendoza R, Cruz I, Lopez C. A Scalable Automated Platform for Immune Tumor Organoids Enables Functional Evaluation of Chemo-Immunotherapy. Interdiscip Res Med Sci Spec. 2026;6(1):1-14. https://doi.org/10.51847/YXM9SQygAQ

Introduction

Chemotherapy and immunotherapy constitute two major therapeutic options for breast cancer [1], although both approaches encounter substantial limitations in clinical use. Patients commonly acquire resistance to treatment agents, leading to diminished therapeutic success. Additionally, many drugs demonstrate efficacy restricted to particular subtypes or disease stages, reflecting the marked heterogeneity of breast cancer and the multifaceted tumor microenvironment [2]. Epirubicin, an anthracycline chemotherapeutic, suppresses cancer cell growth and division through direct DNA intercalation that disrupts DNA synthesis and replication processes. Despite this mechanism, resistance in breast cancer cells severely constrains its practical application [3]. Clinical evidence indicates that tumor-associated macrophages (TAMs) significantly modulate cancer cell drug sensitivity [4], positioning TAMs as a valuable target for immunotherapeutic intervention [5, 6], especially within breast cancer contexts [7]. PLX3397 (pexidartinib) selectively blocks the colony-stimulating factor 1 (CSF1) receptor, thereby interrupting CSF1-dependent signaling essential for TAMs proliferation, maturation, and viability [8]. This

property supports its potential use in combination regimens to counteract TAMs-driven resistance and enhance overall treatment effectiveness against breast cancer.

Standard preclinical drug evaluation typically begins with two-dimensional cell culture models exposed to candidate compounds to select agents showing strong anticancer activity with acceptable selectivity over normal cells. Promising candidates then undergo further testing in animal models to determine in vivo efficacy, safety, and pharmacokinetic behavior [9]. Nevertheless, roughly 90% of such candidates ultimately fail to progress to human clinical trials despite extensive preclinical assessment [10]. The advent of tumor organoid technology has provided a more physiologically relevant platform capable of mirroring key architectural and transcriptional features of native tumors [11]. Existing studies confirm that organoids can accurately predict patient responses to chemotherapy, targeted agents, and combination therapies [12, 13]. Although reliable breast cancer organoid platforms were introduced in 2018 [14], ongoing research has emphasized the development of improved co-culture systems integrating immune cells with cancer cells, utilizing either native or engineered tumor microenvironment (TME) models [15]. Native TME approaches, including air-liquid interface (ALI) and microfluidic three-dimensional cultures, maintain intact tumor fragments together with their original microenvironment [16]. However, adapting ALI methods specifically for breast organoids has proven particularly demanding due to difficulties in sustaining organoid expansion and immune cell viability compared with other cancer types. Microfluidic systems, while commercially accessible in some forms, demand considerable technical skill because of their intricate setup and inconsistent reproducibility [17]. In contrast, Matrigel-based reconstructed TME models involve adding isolated or cultured immune cells to breast cancer cells embedded in Matrigel. A key drawback is the frequent loss of immune components during tissue dissociation. In breast cancer, M2-polarized TAMs may represent up to 50% of the cellular composition in certain solid tumors, actively fostering tumor expansion, dampening immune surveillance, and promoting drug-resistant stem-like properties [18]. Without TAMs, Matrigel organoids struggle to model the activity of clinically relevant agents such as PLX3397, thereby limiting their usefulness for studying combined chemo-immunotherapy.

Our prior work established alginate cryogels with controllable pore dimensions and porosity levels. Cryogels exhibiting larger pores or elevated porosity were found to drive M2 macrophage polarization and promote anti-inflammatory activity, indicating that these materials can mimic a supportive fibrillar extracellular matrix (ECM) favorable for M2-type TAMs development [19]. Building upon this, a subsequent investigation [20] employed the system to create immunized tumor organoids via co-culture of breast cancer cells and TAMs. Results showed that the TAMs-enriched immune milieu substantially accelerated organoid proliferation and enhanced malignant characteristics in vitro. While this model provided long-term culture stability, bulk culture formats were unsuitable for scaled drug screening. The current study therefore introduces an accessible automated multi-well platform for scalable production of these co-culture organoids. This platform enables systematic evaluation of epirubicin and PLX3397 combination therapy while facilitating mechanistic exploration of TAMs-associated drug resistance.

Materials and Methods

Cells and materials

MCF-7 cells (a human breast cancer cell line) were maintained in RPMI 1640 medium supplemented with 10% fetal bovine serum and 1% penicillin G and streptomycin. Human THP-1 cells were differentiated into macrophage-like cells by exposure to 50 nM phorbol 12-myristate 13-acetate (PMA, Sigma) for 3 days. Alginates (5−40 mPa s) were sourced from Aladdin (China). Epirubicin and PLX3397 were acquired from MCE (China). CCK-8 and calcein-AM reagents were obtained from Solarbio (China).

Fabrication of breast cancer organoids in an automated robotic microinjection system

As depicted in Scheme 1, a 2% (w/v) alginate solution was prepared in ddH_2O and loaded into the sample reservoir. The automated robotic arm aspirated 100 μL per channel and delivered this volume into 96-well culture plates containing 2% $CaCl_2$ solution. Ionic cross-linking occurred during a 1 h incubation, forming hydrogels in situ, which were subsequently washed with deionized water. Cryogels were produced by freezing the hydrogels at −80°C for 4 h, followed by lyophilization for 12 h. Suspensions of MCF-7 cells and macrophages were prepared at a final density of 5×10^4 cells/mL. These mixed suspensions were added dropwise onto the porous cryogels in the 96-well plates and permitted to infiltrate fully over a 30 min period. The plates were then placed in a 37°C

incubator with a humidified 5% CO_2 atmosphere. Macrophage polarization was induced by supplementing the culture medium with 20 ng/mL IL-4 (PeproTech) for the first 48 h.

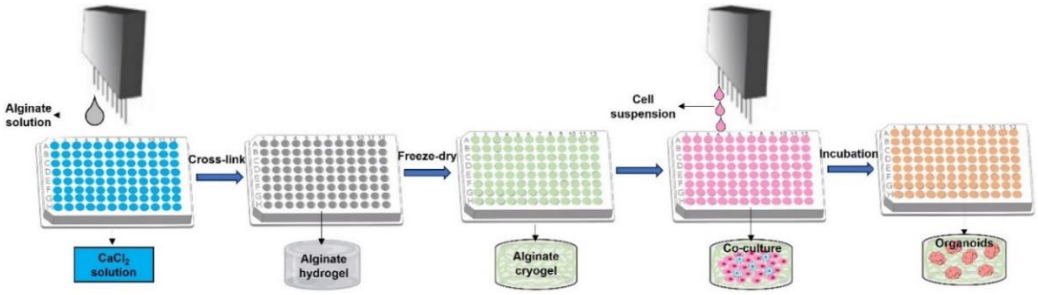

Scheme 1. Production of breast cancer organoids via an automated robotic microinjection system.

SEM observation

After culture, the hydrogels were rinsed twice with PBS and fixed in 2.5% glutaraldehyde for 1 h. The specimens were washed again with phosphate buffer saline (PBS) and pre-frozen at −80°C for 12 h. Cross-sections of the samples were coated with gold for about 90 s and imaged using a scanning electron microscope (Zeiss, Gemini300).

Cell viability assay

Scaffolds were exposed to 10% CCK-8 solution (Dojindo, China) for 4 h at 37°C. Absorbance was measured at 450 nm using a Multimode Microplate Reader (Synergy2, Bio Tek, USA). IC_{50} values were computed with Prism software. Cell viability indices and Combination Index (CI) values were determined using CompuSyn software.

Live and dead assay

Samples were washed with PBS and stained with calcein AM/PI solution at room temperature for 20 min while protected from light. After additional PBS washes, the cut surfaces were examined under an inverted fluorescence microscope. Green fluorescence marked live cells, and red fluorescence indicated dead cells.

Enzyme-Linked Immunosorbent Assay (ELISA)

Supernatants were harvested after 7 days from breast cancer organoids cultured in the presence or absence of macrophages, along with macrophage monocultures. Concentrations of IL10, TGF-β, CCL17, CCL24, vascular endothelial growth factor (VEGF), and EGF were quantified following the supplier's protocol (MultiSciences, China). Absorbance readings were taken at 450 nm on a microplate reader and adjusted against the 570 nm reference wavelength.

Transwell assay

Organoids cultured with or without macrophages were retrieved from the alginate cryogels, dissociated into single-cell suspensions of uniform density, and loaded into Transwell inserts (Corning). For invasion experiments, Transwell membranes were pre-coated with Matrigel prior to cell seeding. Complete growth medium containing serum was added to the lower compartment to stimulate migration. Following 3 days of incubation, migrated cells on the underside of the membrane were fixed with paraformaldehyde. Cells remaining on the upper surface were carefully wiped away with a cotton swab. Migrated cells were stained with 0.2% crystal violet and examined microscopically.

RNA sequencing analysis

RNA was extracted and purified via oligo(dT)-linked magnetic beads before fragmentation. Double-stranded cDNA was synthesized, end-repaired, and ligated with sequencing adapters. PCR amplification generated the final library, which was sequenced on a BGIseq500 platform (BGI-Shenzhen, China). Bioinformatic processing of RNA-seq results was conducted using Dr. Tom (https://biosys.bgi.com), and Kyoto Encyclopedia of Genes and Genomes (KEGG) pathway enrichment was analyzed with DESeq2 software.

Quantitative real-time PCR (qRT-PCR)

Samples were collected, washed with PBS, and processed for total RNA isolation using Trizol reagent (Yeason, China). 1000 ng of RNA per sample was reverse-transcribed to cDNA (Vazyme, China). Quantitative real-time PCR was carried out with the Taq Pro Universal SYBR system (Vazyme, China). Relative expression levels were determined by the $-2\Delta\Delta Ct$ method.

Statistical analysis

Statistical evaluations were performed in Origin 9.0 software employing one-way ANOVA or Student's t-test. Differences were regarded as significant at $p < 0.05$. Experimental results are reported as mean value ± standard deviation.

Results and Discussion

Fabrication of immunized breast cancer organoids in ECM-mimicked hydrogels

The establishment of a three-dimensional matrix capable of supporting spheroid formation and serving as a reliable platform for pharmacological screening was essential. Cryogels represent a specialized category of hydrogels formed through polymerization under subzero conditions. These materials possess a highly macroporous structure that combines elevated porosity with robust mechanical integrity, thereby providing an environment conducive to spheroid development within a simulated tumor microenvironment [21, 22]. A primary aim of this investigation was to assess the performance of the newly developed tumor organoid system relative to conventional culture techniques, including standard hydrogels and multi-well formats. To achieve this, an automated robotic microinjection system **(Figure 1a)** was utilized for two key functions: the in situ generation of alginate hydrogels and the precise delivery of mixed cell suspensions containing breast cancer cells and TAMs to produce organoids.

The alginate hydrogels self-assembled within multi-well plates upon exposure to $CaCl_2$ solution through calcium ion-mediated cross-linking over a 1 h period **(Figure 1b)**. Subsequent freeze-drying yielded alginate cryogels displaying an interconnected porous network **(Figure 1c)**. The mean pore diameter measured 181.5 ± 49.8 μm, with a porosity of 66.5% ± 9.4%, consistent with findings from earlier reports [19, 20]. These characteristics demonstrate the capacity of the cryogels to emulate the structural features of the extracellular matrix in vitro.

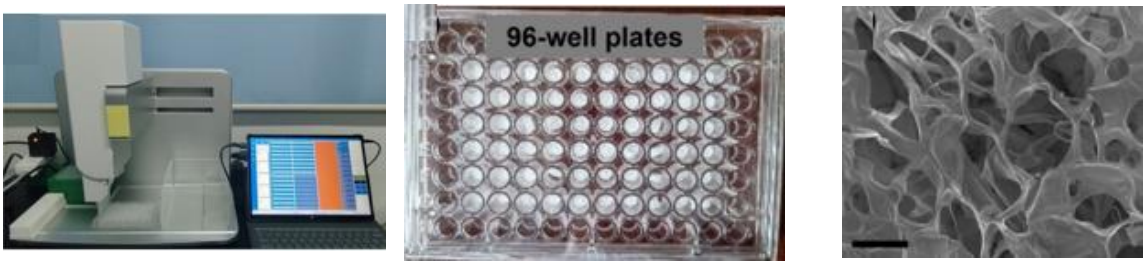

a) b) c)

Figure 1. (a) Automated robotic microinjection system. (b) Alginate cryogels generated in situ. (c) Scanning electron micrograph showing the pore structure of alginate cryogel, scale bar: 100 μm.

To characterize the mechanical properties of the alginate cryogels, five randomly selected samples from a single 96-well plate were subjected to compression testing and Young's modulus determination. The resulting compressive stress-strain profiles revealed consistent plastic deformation beyond 60% strain **(Figure 2a)**, while Young's moduli across the five hydrogels remained comparable, averaging approximately 100 kPa **(Figure 2b)**. Following 30 min of cell suspension seeding, adherent cells and cell clusters were readily visible on both the surface and interior of the cryogels **(Figure 2c)**. These observations align with previous findings [19, 20] and confirm that the microinjection platform reliably reproduces the physical and mechanical attributes of alginate cryogels suitable for tumor organoid cultivation.

Co-culture of breast cancer cells and TAMs within the alginate cryogels successfully established a TAMs-dominated immune microenvironment that promoted breast cancer organoid development. Live/dead staining demonstrated high cell viability of 96.7 ± 3.3% **(Figure 2d)**. After 7 days of culture, numerous compact spheroids with diameters of approximately 100 μm had formed **(Figures 2e and 2f)**. Macrophage polarization status was evaluated through immunofluorescent labeling of CD86 (M1 marker) and CD163 (M2 marker). The results

indicated predominant M2 polarization within the spheroids, mirroring the in vivo situation in which M2-type TAMs can comprise up to 50% of the cellular population in certain solid tumors [18]. Scanning electron microscopy further revealed well-developed spheroids integrated within the alginate cryogel matrix **(Figure 2g)**, suggesting active cell–ECM interactions.

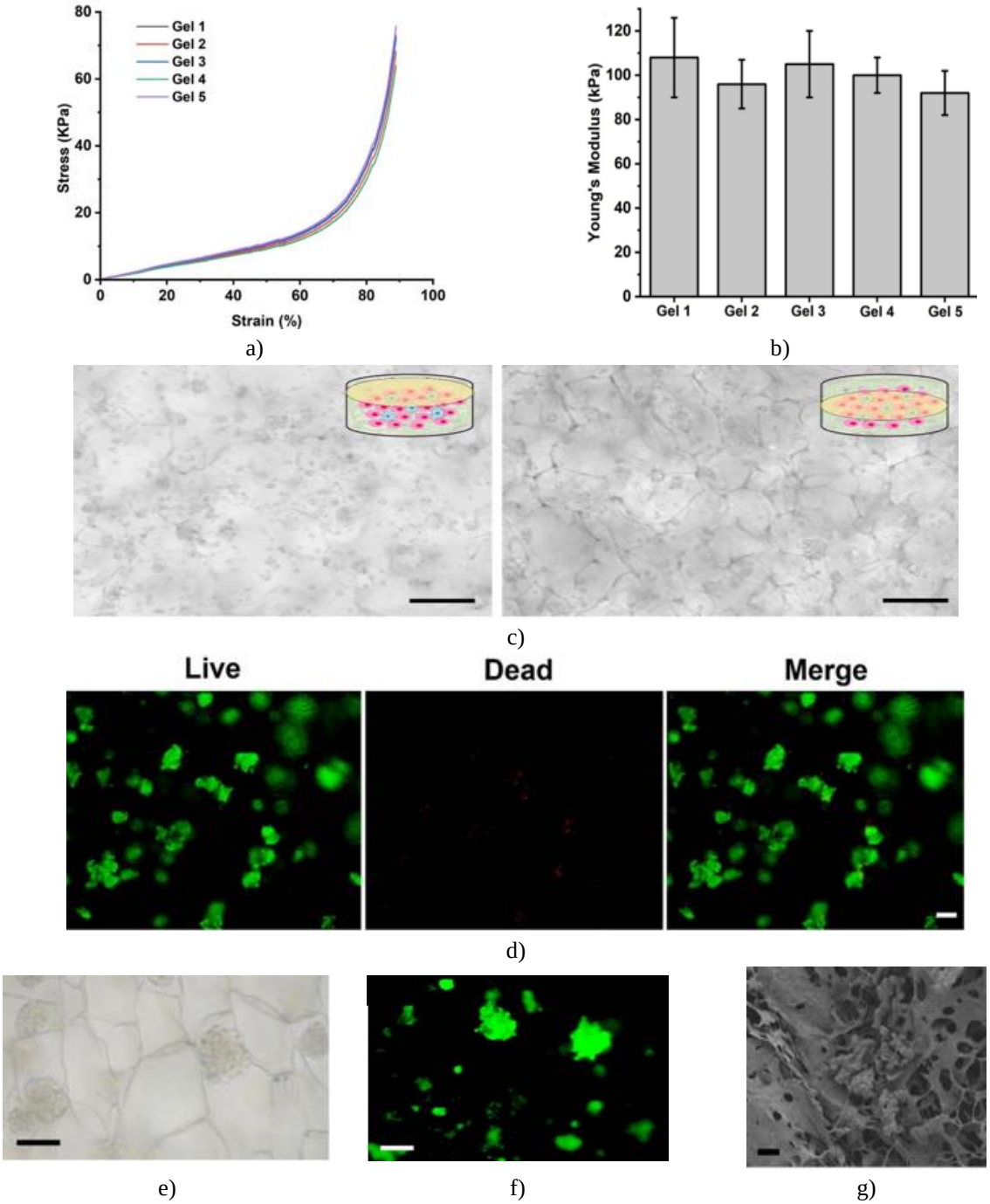

Figure 2. Compressive stress-strain curve (a) and Young's moduli (b) of alginate cryogels. Representative images showing the surface and interior of cryogels 30 min after cell seeding (c). Fluorescent live/dead staining (d), bright-field image (e), fluorescent image (f), and scanning electron micrograph (g) of spheroids formed inside alginate hydrogels following 7-day culture. Scale bar: 100 μm.

Assessment of chem-immunotherapy using epirubicin in combination with PLX3397

Patients with breast cancer commonly develop resistance to epirubicin. Moreover, the emergence of this resistance in breast cancer cells is challenging to detect using standard in vitro models, which restricts the reliability of anticancer drug screening. In the present work, we investigated variations in epirubicin sensitivity across breast

cancer organoid cultures maintained with and without tumor-associated macrophages (TAMs), alongside spheroids formed exclusively from TAMs. As presented in **Figure 3a**, responses to epirubicin remained largely comparable among the three groups at lower drug concentrations. At elevated concentrations, however, the presence of TAMs led to substantially heightened resistance relative to the control conditions. This pattern was corroborated by the corresponding IC50 values: 153.9 ± 27.7 nM for breast cancer organoids without TAMs, 157.2 ± 35.8 nM for TAMs alone, and 701.6 ± 107.6 nM for breast cancer organoids with TAMs. Overall, inclusion of TAMs within the organoids increased resistance to epirubicin by roughly 4.7 times. These observations imply that TAMs play a central role in fostering drug resistance in breast cancer organoids cultured in biomimetic environments, aligning with their established tumor-supportive properties in living systems [18].

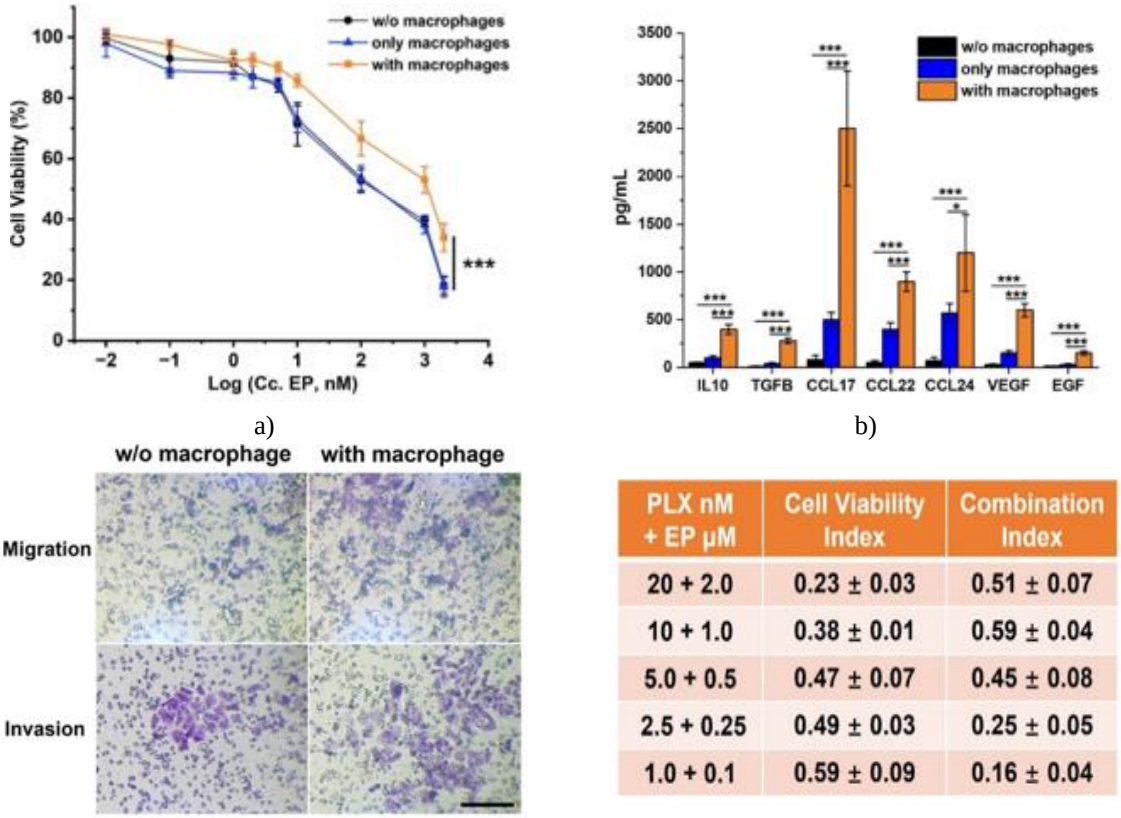

PLX nM + EP µM	Cell Viability Index	Combination Index
20 + 2.0	0.23 ± 0.03	0.51 ± 0.07
10 + 1.0	0.38 ± 0.01	0.59 ± 0.04
5.0 + 0.5	0.47 ± 0.07	0.45 ± 0.08
2.5 + 0.25	0.49 ± 0.03	0.25 ± 0.05
1.0 + 0.1	0.59 ± 0.09	0.16 ± 0.04

d)

Figure 3. (a) Cell viability responses to epirubicin in breast cancer organoids cultured with or without macrophages, and in macrophages alone. (b) ELISA quantification of secreted cytokines in breast cancer organoids cultured with or without macrophages, and in macrophages alone. : *p < 0.05, ***p < 0.001. (c) Transwell migration (upper) and invasion (lower) assays performed on breast cancer cells derived from organoids with and without macrophages. Bright-field images were acquired at day 3 with an inverted microscope; scale bar: 100 µm. (d) Cell viability and combination index values for different pairings of PLX3397 and epirubicin. EP: epirubicin, PLX: PLX3397.

ELISA analysis revealed significantly elevated secretion of several critical cytokines involved in intercellular signaling and immune modulation within breast cancer organoids containing macrophages **(Figure 3b)**. These included the chemokines CCL17, CCL22, and CCL24, the immunosuppressive cytokines IL-10 and TGF-β, and the growth factors VEGF and EGF. Prior studies have established that IL-10 and TGF-β strengthen the immunosuppressive milieu within tumors [23]. M2-polarized macrophages have also been linked to diminished paclitaxel effectiveness in breast cancer through activation of the IL-10/STAT3/Bcl-2 pathway [24]. Additionally, CCL22 produced by M2-like TAMs can impair sensitivity to 5-FU by triggering EMT, activating PI3K/Akt signaling, and blocking caspase-dependent apoptosis [25]. VEGF facilitates M2-like macrophage polarization while cooperating with these cells to stimulate angiogenesis in poorly vascularized tumors, potentially hindering efficient drug delivery and elevating tumor tolerance to treatment [26]. EGF, in turn, activates JAK/STAT3 signaling, promotes M2-like polarization, and contributes to resistance against osimertinib [27]. Transwell

experiments further demonstrated that macrophages markedly enhanced the migratory and invasive capabilities of breast cancer cells within the organoids, as indicated by increased cell movement after three days **(Figure 3c)**. To counteract drug resistance observed in the co-culture setting, subsequent experiments explored the use of PLX3397, a macrophage-directed agent, to suppress TAM function within the biomimetic matrix. Therapeutic outcomes were compared among epirubicin alone, PLX3397 alone, and the dual-drug regimen in breast cancer organoids harboring TAMs. Combination index (CI) calculations were performed across a range of concentrations to evaluate the nature of drug interactions. Results shown in **Figure 3d** indicated that all CI values for the combination treatments fell below 0.75, confirming strong synergistic interactions between the macrophage-targeted agent PLX3397 and the chemotherapeutic drug epirubicin. Collectively, these data highlight how cytokine secretion in macrophage-enriched tumor organoids contributes to more aggressive malignant behavior and increased chemoresistance.

Live-dead staining was additionally employed to directly visualize cell viability and treatment responses within the three-dimensional matrix **(Figure 4a)**. Consistent with its selective action on TAMs, PLX3397 monotherapy produced almost no cytotoxic impact on the breast cancer organoids compared with untreated controls (BK). Epirubicin monotherapy induced clear cell death, predominantly affecting cells on the organoid periphery (red signal). The combined regimen (Mix) yielded the most potent cytotoxicity, with dead cells evident even in deeper regions of the organoids. Quantitative assessment confirmed a significantly higher proportion of dead cells in the Mix group than in the epirubicin-only group. In organoids lacking TAMs, the killing efficiency of the combination and epirubicin alone was equivalent. Immunostaining for cell-type-specific markers (CD163 for M2-type TAMs and CD133 for breast cancer cells) was used to track shifts in cellular composition **(Figure 4b)**. Control organoids contained roughly equal proportions of breast cancer cells and macrophages. PLX3397 treatment substantially reduced the macrophage fraction, elevating the breast cancer cell proportion to 76.2% ± 7.3%. Epirubicin, acting as a non-selective cytotoxic agent, decreased overall organoid size but did not markedly alter the relative abundance of the two cell populations. In the combination arm, dual depletion of macrophages by both agents resulted in the highest breast cancer cell fraction of 85.1% ± 8.2%.

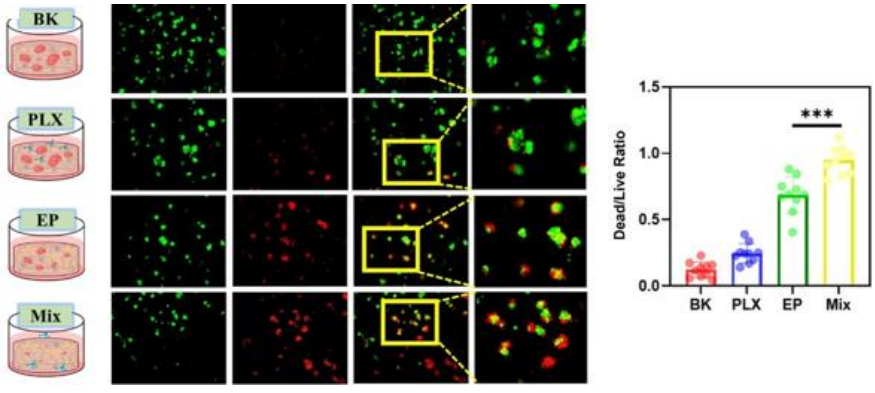

a)

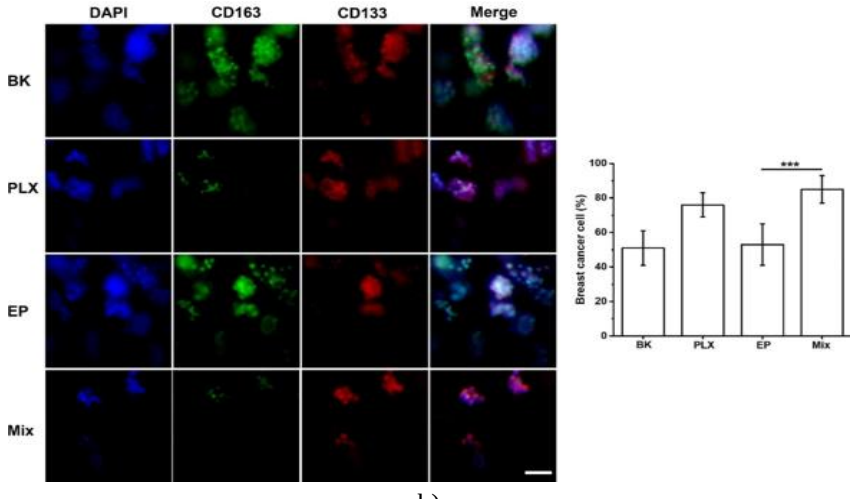

b)

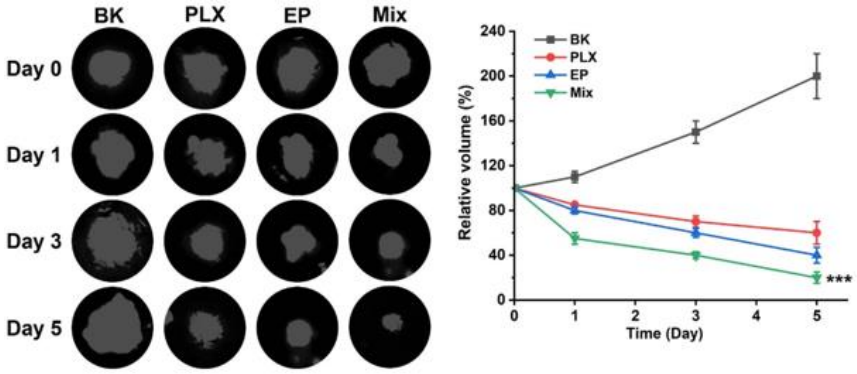

c)

Figure 4. (a) Live/dead staining of breast cancer organoids containing macrophages under different treatment conditions, with quantification of dead-to-live cell ratios. (b) Fluorescence images of co-cultures showing TAMs (CD163, green) and MCF-7 breast cancer cells (CD133, red), with DAPI nuclear counterstaining (blue). Scale bar: 100 μm. Percentages of breast cancer cells within organoids were determined. (c) Assessment of growth suppression in breast cancer organoids following various treatments. Drug-free medium served as the control. Relative organoid volumes at different time points are normalized to day 0 values. BK: untreated control, PLX: PLX3397 alone, EP: epirubicin alone, Mix: PLX3397 plus epirubicin. : ***$p < 0.001$.

Growth dynamics of the organoids were monitored across treatment groups **(Figure 4c)**. Untreated controls exhibited continuous expansion, attaining nearly 200% of starting volume by day 5. Both PLX and EP monotherapies produced moderate volume reductions to approximately 60% and 40% of initial size, respectively. The combination treatment achieved superior inhibition, decreasing organoid volume to about 20% of the original. Histological sections from day 0 and day 5 corroborated these differential inhibitory effects. Calculation of the time required for organoid volume to decline to 50% of baseline (T1/2) yielded 3.94 ± 0.55 days for epirubicin alone and 1.68 ± 0.37 days for the combination. These results underscore the enhanced therapeutic impact of dual treatment, attributable to decreased drug resistance and deeper penetration of the chemotherapeutic agent following TAM depletion.

Mechanistic exploration of drug resistance reversal via combined therapy

To elucidate the mechanisms underlying the reversal of drug resistance in breast cancer cells through combined treatment, transcriptomic profiling via RNA sequencing was performed on samples subjected to the different therapeutic regimens. The analysis identified 255 differentially expressed genes in the combination therapy group **(Figure 5a)**, 246 genes following PLX3397 monotherapy, 768 genes after epirubicin monotherapy, and 11 genes that were commonly altered across all treatment arms (ATP5MF, FUT9, TEX49, CDRT4, H3C15, ZNF81, DDR2, NUTM2A, TBC1D3H, FMNL1, CACNB4). Subsequent KEGG pathway enrichment analysis **(Figure 5b)** identified the five most prominent pathways: cytokine-cytokine receptor interaction, mitogen-activated protein kinase (MAPK) signaling pathway, PI3K-Akt signaling pathway, epidermal growth factor receptor (EGFR) tyrosine kinase inhibitor resistance, and ECM-receptor interaction. Corresponding heat maps **(Figure 5c)** highlighted the specific differentially expressed genes within each of these pathways, many of which are known to contribute to chemoresistance in breast cancer.

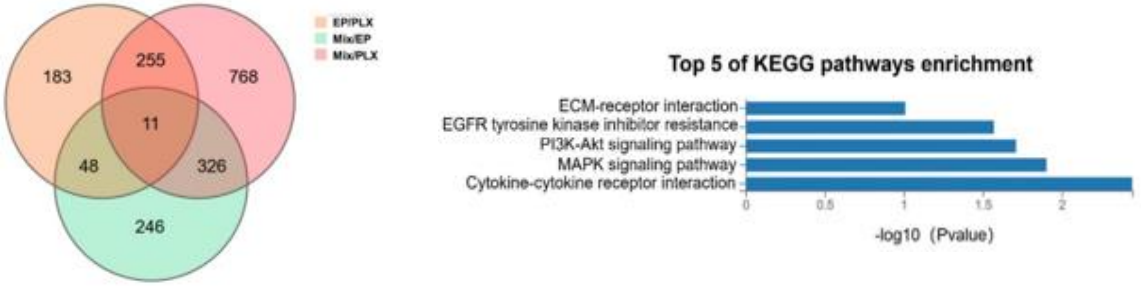

a) b)

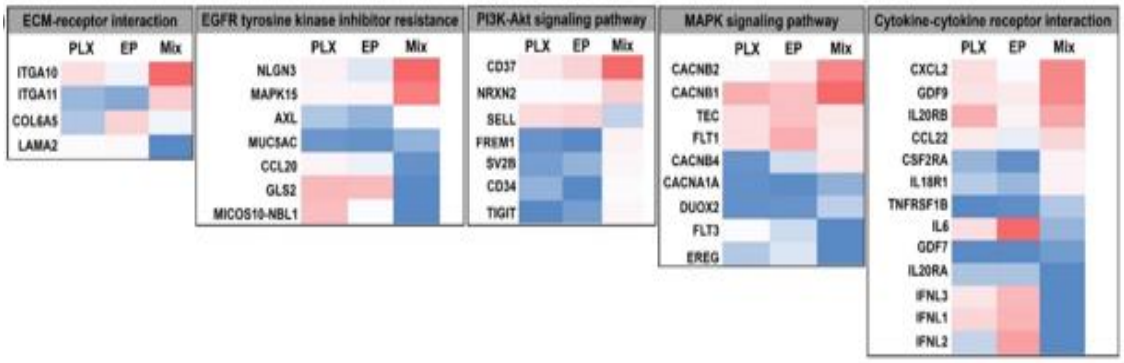

c)

Figure 5. Overview of global transcriptomic alterations. (a) Venn diagram depicting the distribution of differentially expressed genes among treatment conditions. (b) KEGG enrichment analysis indicating the top five enriched pathways. (c) Heat maps showing differentially expressed genes associated with ECM-receptor interaction, EGFR tyrosine kinase inhibitor resistance, PI3K-Akt signaling pathway, MAPK signaling pathway, and cytokine-cytokine receptor interaction. PLX: PLX3397 monotherapy, EP: epirubicin monotherapy, Mix: co-administration of PLX3397 and epirubicin.

Based on these transcriptomic findings, three candidate genes—IL6, CD37, and GLS2—were chosen for detailed investigation owing to their notable expression differences across the treatment groups. These genes map to the cytokine-cytokine receptor interaction, PI3K-Akt signaling pathway, and EGFR tyrosine kinase inhibitor resistance pathways, respectively. Quantitative real-time PCR was then used to measure their mRNA levels in each experimental condition **(Figure 6a)**. Combination therapy led to a pronounced reduction in IL6 expression. As IL6 is known to facilitate tumor immune escape and promote chemoresistance [28], its downregulation via macrophage-directed combination approaches may enhance the responsiveness of breast cancer cells to chemotherapy. Conversely, CD37 mRNA levels were significantly elevated in the combination treatment group. Prior evidence indicates that diminished CD37 expression correlates with the acquisition of drug resistance in tumors [29]; therefore, its upregulation during combined therapy could aid in restoring drug sensitivity in breast cancer cells. Furthermore, GLS2 expression is typically induced under chemotherapeutic stress in cancer cells [30]. In this study, the dual treatment effectively suppressed this stress-related increase in GLS2, pointing to an additional mechanism for attenuating resistance. Functional assays revealed that modulation of IL6, CD37, and GLS2 expression markedly affected the improved cell-killing efficacy achieved by co-administration in the immune-reconstituted tumor organoid system **(Figure 6b)**. Addition of IL6 or suppression of CD37 resulted in elevated macrophage proportions and reduced breast cancer cell fractions within the organoids, while GLS2 inhibition produced a slight rise in the breast cancer cell percentage.

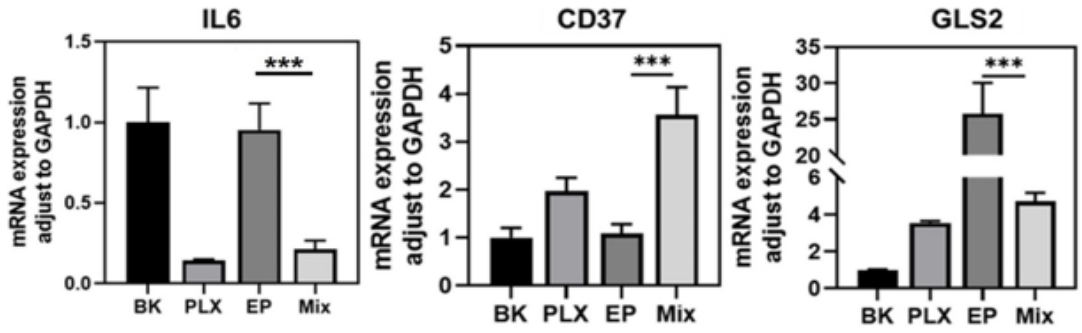

a)

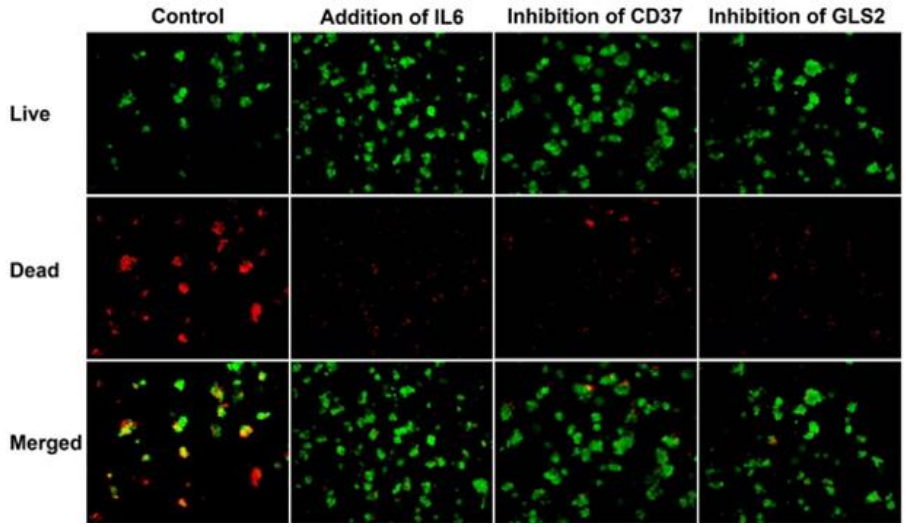

b)

Figure 6. (a) Quantitative analysis of IL6, CD37, and GLS2 mRNA expression in macrophage-containing breast cancer organoids following various treatments by qRT-PCR. : ***p < 0.001. (b) Live/dead cell staining evaluating organoid responses to combined PLX3397 and epirubicin therapy under altered expression of the three target factors.

Breast cancer commonly acquires resistance to chemotherapeutic drugs and is particularly difficult to manage once it reaches advanced or metastatic stages [31]. Although immunotherapeutic agents have shown strong promise across multiple cancer types, their efficacy as standalone treatments remains limited [32]. In breast cancer, the tumor microenvironment (TME) significantly influences both disease progression and resistance to therapy. M2-polarized tumor-associated macrophages (TAMs) can account for up to 50% of the cellular content in some solid tumors and help establish an immunosuppressive milieu that promotes tumor persistence [18]. The extracellular matrix (ECM) additionally acts as a physical obstacle, restricting the access of immune effector cells and chemotherapeutic agents [33]. Therefore, the development of 3D organoid models that accurately replicate this immunosuppressive TME is vital for effective drug screening in the context of chemo-immunotherapy [34].
The present study utilized a TAMs-integrated organoid model that closely mirrored the biological features of the source tumors and successfully recreated an immunosuppressive niche, as previously confirmed in our recent work [20]. Alginate hydrogels were employed in this culture system to provide a three-dimensional scaffold supporting cell adhesion, while eliminating the risk of zoonotic pathogen transmission inherent to Matrigel, which can adversely affect macrophage behavior [35]. These hydrogels further contributed to a physiologically relevant 3D setting that better preserves the architectural organization of original tumor tissue [36]. Moreover, the scaffold structure within the organoids served as a barrier that limited drug penetration, thereby enhancing the model's ability to simulate realistic responses to chemo-immunotherapeutic interventions.
Tumor organoid technology has emerged as a key innovation propelling precision medicine forward by supplying clinically more relevant platforms for testing therapeutic strategies and potentially improving patient outcomes [37]. Microfabricated microwell systems have demonstrated utility as alternatives to traditional bulk culture approaches and are extensively used in tissue engineering for three-dimensional cell cultivation [38-40]. Despite these advances, tumor organoids frequently suffer from high variability and limited reproducibility arising from differences in culture protocols and conditions, which hinders their standardization for chemo-immunotherapy testing. To reliably capture tumor heterogeneity and reduce technical inconsistencies, a robust and standardized culture platform is required. Accordingly, we present a user-friendly automated microwell platform designed for high-throughput production of tumor organoids, allowing selective retrieval of individual organoids for further molecular analysis. This automated system provides several distinct advantages over conventional methods. Unlike bulk cultures, the microwell format permits accurate assessment of quantitative traits at the single-organoid level rather than relying on population averages [41], including growth dynamics and drug sensitivity **(Figure 4c)**. In contrast to closed microfluidic platforms that depend on costly specialized equipment such as custom chips and peristaltic pumps [42, 43], our microwell arrays are compatible with standard commercial 48- or 96-well plates, and the robotic microinjection system integrates smoothly into existing cell culture workflows **(Scheme 1**

and Figure 1). The platform also achieves comparable throughput, supporting the simultaneous generation of 96 organoid samples in a 96-well plate, on par with other established techniques that handle roughly one hundred organoids [44, 45]. Consequently, this automated robotic microinjection platform offers a reproducible framework with sufficient sample volume for robust comparison of experimental data and clinical treatment responses. Building upon our earlier direct co-culture model of breast cancer cells and TAMs that recapitulated intercellular and cell–matrix interactions [20], the current study introduces an optimized organoid system generated entirely within the automated microinjection platform. This enables in situ hydrogel formation and uniform cell seeding, facilitating high-throughput screening and improved prediction of clinical outcomes in breast cancer chemo-immunotherapy.

Although substantial progress has been made in understanding cancer biology and developing new therapies, cancer continues to rank as the second leading cause of death worldwide [46]. A central contributor to treatment failure is the tumor's capacity to evade immune detection and acquire resistance to administered drugs [47]. Investigating how cancer cells modulate immune responses during the development of chemotherapy resistance is therefore critical. In this work, we evaluated the combination of PLX3397 with the standard chemotherapeutic drug epirubicin. We first observed that the inclusion of TAMs in the biomimetic matrix significantly enhanced breast cancer cell resistance to epirubicin, reflected by a 4.7-fold rise in IC50 values in TAM-containing organoids compared with TAM-free controls **(Figure 3a)**. While PLX3397 alone exhibited minimal direct cytotoxicity toward breast cancer organoids, it effectively alleviated the TAM-driven immunosuppressive conditions and markedly improved chemotherapeutic performance when used in combination **(Figure 4)**. This synergy was quantitatively validated through combination index (CI) calculations across five different concentration ratios of PLX3397 and epirubicin **(Figure 3d)**. PLX3397 (pexidartinib), a powerful CSF1R inhibitor, has already gained FDA approval for treating symptomatic tenosynovial giant cell tumors that express CSF1 [8, 48, 49]. Previous research by Yan *et al*. [50] showed that PLX3397 inhibited glioma progression, reduced tumor cell proliferation, and decreased tumor grade by counteracting TME-mediated resistance pathways. The compound disrupted tumor-induced macrophage reprogramming and restored glioma cell sensitivity to tyrosine kinase inhibitors in preclinical models. Similarly, Fujiwara *et al*. [51] demonstrated that PLX3397 suppressed M2 polarization, cell survival, and migratory capacity in bone marrow-derived macrophages. Systemic treatment with PLX3397 in an orthotopic osteosarcoma model substantially reduced primary tumor burden and lung metastases, underscoring its potent macrophage-modulating activity with translational potential for cancer immunotherapy. As a result, TAM-directed inhibitors are gaining prominence in anti-tumor immunity research for their ability to upregulate antigen presentation and costimulatory molecules while altering immune cell behavior via cytokine networks [23, 52, 53]. Developing potent CSF1R inhibitors such as PLX3397 thus represents a valuable approach to interrupting pro-tumorigenic signaling within the TME [8].

Additional analyses were conducted to elucidate the molecular mechanisms associated with immune modulation during combination therapy. KEGG pathway enrichment of RNA sequencing data highlighted significant alterations in several key pathways **(Figure 5)**, notably cytokine–cytokine receptor interaction, PI3K-Akt signaling, and EGFR tyrosine kinase inhibitor resistance. Within these pathways, IL6, CD37, and GLS2 displayed distinct expression profiles in the combination group relative to monotherapy treatments **(Figure 6)**. IL-6 functions as a major regulator of anti-cancer immunity and is frequently upregulated following genotoxic stress. Liu *et al*. [54] reported that IL-6 enhances CSF1R expression and macrophage survival, an effect that can be reversed by PLX3397, suggesting therapeutic relevance for conditions such as clonal hematopoiesis-associated cardiovascular disease. Inhibiting IL-6 may also redirect cancer cell death toward immunogenic pathways, promoting more durable anti-tumor immunity [55]. CD37, a tetraspanin family member, participates in signal transduction cascades that trigger apoptosis through the PI3K-Akt pathway in B-cell malignancies [56]. Elevated CD37 levels have also been linked to increased infiltration of M2 macrophages and neutrophils in gliomas, along with higher expression of immune checkpoint molecules including CD80, CD86, CD276, and PD-L2 [29]. These observations point to promising opportunities for combining CD37-targeted strategies with other immunotherapeutic or kinase inhibitory agents. GLS2 plays a pivotal role in glutamine metabolism and supplies essential carbon and nitrogen resources that drive proliferation in luminal breast cancers [57]. It is also overexpressed in triple-negative breast cancer and metastatic lung cancer and contributes to radio-resistance in advanced cervical cancer, potentially by lowering ROS levels through elevation of GSH, NADH, or NADPH [58-60]. Collectively, these insights into the TME underscore the value of targeting specific metabolic and immune pathways for treating advanced or therapy-resistant cancers [61]. Our findings align with earlier studies and

emphasize the clinical relevance of IL6, CD37, and GLS2 in the context of PLX3397-based chemo-immunotherapy.

Conclusion

This study established a convenient automated multi-well platform using an automated robotic microinjection system to generate TAMs-containing breast cancer organoids embedded in hydrogels that mimic the extracellular matrix. The methodology provided clear benefits over standard bulk culture techniques when evaluating chemo-immunotherapy outcomes. Inclusion of TAMs within the breast cancer organoids led to markedly heightened resistance against epirubicin, a phenotype that was effectively mitigated by the macrophage-targeting agent PLX3397. Combination index (CI) calculations for all tested co-administration conditions demonstrated strong synergistic interactions between epirubicin and PLX3397. The genes IL6, CD37, and GLS2, which exhibited prominent differential expression under combination treatment, participate in the tumor necrosis factor signaling, PI3K-Akt signaling, and EGFR tyrosine kinase inhibitor resistance pathways. These molecules represent compelling candidate targets for advancing future chemo-immunotherapeutic strategies in clinical settings.

Acknowledgments: None

Conflict of Interest: None

Financial Support: None

Ethics Statement: None

References

1. Wilcock P, Webster RM. The breast cancer drug market. Nat Rev Drug Discov. 2021;20(5):339-40.
2. Mehraj U, Dar AH, Wani NA, Mir MA. Tumor microenvironment promotes breast cancer chemoresistance. Cancer Chemother Pharmacol. 2021;87(2):147-58.
3. Khasraw M, Bell R, Dang C. Epirubicin: Is it like doxorubicin in breast cancer? A clinical review. Breast. 2012;21(2):142-9.
4. Xie YT, Yang H, Yang C, He L, Zhang X, Peng L, et al. Role and mechanisms of tumor-associated macrophages in hematological malignancies. Front Oncol. 2022;12:933666.
5. Kennedy LB, Salama AKS. A review of cancer immunotherapy toxicity. CA Cancer J Clin. 2020;70(2):86-104.
6. Vanneman M, Dranoff G. Combining immunotherapy and targeted therapies in cancer treatment. Nat Rev Cancer. 2012;12(4):237-51.
7. Debien V, De Caluwé A, Wang XX, Piccart-Gebhart M, Tuohy VK, Romano E, et al. Immunotherapy in breast cancer: An overview of current strategies and perspectives. NPJ Breast Cancer. 2023;9(1):7.
8. Lamb YN. Pexidartinib: First approval. Drugs. 2019;79(16):1805-12.
9. Zhao Z, Zhang S, Jiang N, Zhu W, Song D, Liu S, et al. Patient-derived immunocompetent tumor organoids: A platform for chemotherapy evaluation in the context of T-cell recognition. Angew Chem Int Ed Engl. 2024;63(9):e202317613.
10. Sharpless NE, DePinho RA. The mighty mouse: Genetically engineered mouse models in cancer drug development. Nat Rev Drug Discov. 2006;5(9):741-54.
11. Drost J, Clevers H. Organoids in cancer research. Nat Rev Cancer. 2018;18(7):407-18.
12. Yin SY, Xi RB, Wu AW, Wang S, Li YJ, Wang CB, et al. Patient-derived tumor-like cell clusters for drug testing in cancer therapy. Sci Transl Med. 2020;12:eaaz1723.
13. Xu H, Jiao D, Liu A, Wu K. Tumor organoids: Applications in cancer modeling and potentials in precision medicine. J Hematol Oncol. 2022;15(1):58.
14. Sachs N, de Ligt J, Kopper O, Gogola E, Bounova G, Weeber F, et al. A living biobank of breast cancer organoids captures disease heterogeneity. Cell. 2018;172(1-2):373-86.
15. Guan DD, Liu XZ, Shi QY, He BJ, Zheng CP, Meng XL. Breast cancer organoids and their applications for precision cancer immunotherapy. World J Surg Oncol. 2023;21(1):343.

16. Yuki K, Cheng N, Nakano M, Kuo CJ. Organoid models of tumor immunology. Trends Immunol. 2020;41(8):652-64.
17. Wakefield L, Agarwal S, Tanner K. Preclinical models for drug discovery for metastatic disease. Cell. 2023;186(8):1792-813.
18. Vitale I, Manic G, Coussens LM, Kroemer G, Galluzzi L. Macrophages and metabolism in the tumor microenvironment. Cell Metab. 2019;30(1):36-50.
19. Liu ZZ, Xu NY, Wang ML, Tang RZ, Liu XQ. Physical confinement in alginate cryogels determines macrophage polarization to a M2 phenotype by regulating a STAT-related mRNA transcription pathway. Biomater Sci. 2022;10(9):2315-27.
20. Xu NY, Li J, Wang ML, Chen XY, Tang R, Liu XQ. Fabrication of a coculture organoid model in the biomimetic matrix of alginate to investigate breast cancer progression in a TAMs-leading immune microenvironment. ACS Appl Mater Interfaces. 2024;16(9):11275-88.
21. Memic A, Colombani T, Eggermont LJ, Rezaeeyazdi M, Steingold J, Rogers ZJ, et al. Latest advances in cryogel technology for biomedical applications. Adv Ther. 2019;2:1800114.
22. Omidian H, Chowdhury SD, Babanejad N. Cryogels: Advancing biomaterials for transformative biomedical applications. Pharmaceutics. 2023;15(7):1836.
23. Wang SJ, Wang JR, Chen ZQ, Luo JM, Guo W, Sun LL, et al. Targeting M2-like tumor-associated macrophages is a potential therapeutic approach to overcome antitumor drug resistance. npj Precis Oncol. 2024;8(1):31.
24. Yang CX, He L, He P, Liu Y, Wang W, He Y, et al. Increased drug resistance in breast cancer by tumor-associated macrophages through IL-10/STAT3/bcl-2 signaling pathway. Med Oncol. 2015;32:14.
25. Wei C, Yang C, Wang S, Shi D, Zhang C, Lin X, et al. M2 macrophages confer resistance to 5-fluorouracil in colorectal cancer through the activation of CCL22/PI3K/AKT signaling. Onco Targets Ther. 2019;12:3051-63.
26. Wheeler KC, Jena MK, Pradhan BS, Nayak N, Das S, Hsu CD, et al. VEGF may contribute to macrophage recruitment and M2 polarization in the decidua. PLoS One. 2018;13(1):e0191040.
27. Sun YT, Dong YT, Liu XJ, Zhang YD, Bai H, Duan JC, et al. Blockade of STAT3/IL-4 overcomes EGFR T790M-cis-L792F-induced resistance to osimertinib via suppressing M2 macrophages polarization. EBioMedicine. 2022;83:104200.
28. Kumari N, Dwarakanath BS, Das A, Bhatt AN. Role of interleukin-6 in cancer progression and therapeutic resistance. Tumour Biol. 2016;37(9):11553-72.
29. Yan X, Zhou Q, Zhu H, Liu W, Xu H, Yin W, et al. The clinical features, prognostic significance, and immune heterogeneity of CD37 in diffuse gliomas. iScience. 2021;24(11):103249.
30. Altman BJ, Stine ZE, Dang CV. From Krebs to clinic: Glutamine metabolism to cancer therapy. Nat Rev Cancer. 2016;16(10):619-34.
31. Prihantono, Faruk M. Breast cancer resistance to chemotherapy: When should we suspect it and how can we prevent it?. Ann Med Surg (Lond). 2021;70:102793.
32. Vasan N, Baselga J, Hyman DM. A view on drug resistance in cancer. Nature. 2019;575(7782):299-309.
33. Yuan Z, Li Y, Zhang S, Wang X, Dou H, Yu X, et al. Extracellular matrix remodeling in tumor progression and immune escape: From mechanisms to treatments. Mol Cancer. 2023;22(1):48.
34. Kidd BA, Wroblewska A, Boland MR, Agudo J, Merad M, Tatonetti NP, et al. Mapping the effects of drugs on the immune system. Nat Biotechnol. 2016;34(1):47-54.
35. Kim S, Min S, Choi YS, Jo SH, Jung JH, Han K, et al. Tissue extracellular matrix hydrogels as alternatives to Matrigel for culturing gastrointestinal organoids. Nat Commun. 2022;13:1692.
36. Bonani W, Cagol N, Maniglio D. Alginate hydrogels: A tool for 3D cell encapsulation, tissue engineering, and biofabrication. Adv Exp Med Biol. 2020;1250:49-61. doi:10.1007/978-981-15-3262-7_4
37. Zhou Z, Van der Jeught K, Li Y, Sharma S, Yu T, Moulana I, et al. A T cell-engaging tumor organoid platform for pancreatic cancer immunotherapy. Adv Sci (Weinh). 2023;10:e2300548. doi:10.1002/advs.202300548
38. Brandenberg N, Hoehnel S, Kuttler F, Homicsko K, Ceroni C, Ringel T, et al. High-throughput automated organoid culture via stem-cell aggregation in microcavity arrays. Nat Biomed Eng. 2020;4:863-74.
39. Kakni P, Hueber R, Knoops K, López-Iglesias C, Truckenmüller R, Habibovic P, et al. Intestinal organoid culture in polymer film-based microwell arrays. Adv Biosyst. 2020;4(10):e2000126.

40. Shin HS, Hong HJ, Koh WG, Lim JY. Organotypic 3D culture in nanoscaffold microwells supports salivary gland stem-cell-based organization. ACS Biomater Sci Eng. 2018;4(12):4311-20. doi:10.1021/acsbiomaterials.8b00894
41. Yi SA, Zhang YX, Rathnam C, Pongkulapa T, Lee KB. Bioengineering approaches for the advanced organoid research. Adv Mater. 2021;33(45):e2007949. doi:10.1002/adma.202007949
42. Stern A, Thompson B, Williams K, McClellan R, Gebhart S, Hartman J. The CellRaft AIR® system: A novel system enabling organoid imaging, identification, and isolation. SLAS Discov. 2022;27(3):201-8. doi:10.1016/j.slasd.2021.11.003
43. Beghin A, Grenci G, Sahni G, Guo S, Rajendiran H, Delaire T, et al. Automated high-speed 3D imaging of organoid cultures with multi-scale phenotypic quantification. Nat Methods. 2022;19:881-92.
44. Giger S, Hofer M, Miljkovic-Licina M, Hoehnel S, Brandenberg N, Guiet R, et al. Microarrayed human bone marrow organoids for modeling blood stem cell dynamics. APL Bioeng. 2022;6(3):036101. doi:10.1063/5.0092860
45. Wu Y, Li K, Li Y, Sun T, Liu C, Dong C, et al. Grouped-seq for integrated phenotypic and transcriptomic screening of patient-derived tumor organoids. Nucleic Acids Res. 2022;50(5):e28. doi:10.1093/nar/gkab1201
46. The global challenge of cancer. Nat Cancer. 2020;1:1–2. doi:10.1038/s43018-019-0023-9
47. Skirzynska A, Xue C, Shoichet MS. Engineering biomaterials to model immune-tumor interactions in vitro. Adv Mater. 2024;36(19):e2310637. doi:10.1002/adma.202310637
48. Tap WD, Wainberg ZA, Anthony SP, Ibrahim PN, Zhang C, Healey JH, et al. Structure-guided blockade of CSF1R kinase in tenosynovial giant-cell tumor. N Engl J Med. 2015;373(5):428-37. doi:10.1056/NEJMoa1411366
49. Tap WD, Gelderblom H, Palmerini E, Desai J, Bauer S, Blay JY, et al. Pexidartinib versus placebo for advanced tenosynovial giant cell tumour (ENLIVEN): a randomised phase 3 trial. Lancet. 2019;394(10197):478-87. doi:10.1016/S0140-6736(19)30764-0
50. Yan D, Kowal J, Akkari L, Schuhmacher AJ, Huse JT, West BL, et al. Inhibition of colony stimulating factor-1 receptor abrogates microenvironment-mediated therapeutic resistance in gliomas. Oncogene. 2017;36:6049-58.
51. Fujiwara T, Yakoub MA, Chandler A, Christ AB, Yang G, Ouerfelli O, et al. CSF1/CSF1R signaling inhibitor pexidartinib (PLX3397) reprograms tumor-associated macrophages and stimulates T-cell infiltration in the sarcoma microenvironment. Mol Cancer Ther. 2021;20(8):1388-99. doi:10.1158/1535-7163.MCT-20-0591
52. Xiang X, Wang J, Lu D, Xu X. Targeting tumor-associated macrophages to synergize tumor immunotherapy. Signal Transduct Target Ther. 2021;6:75.
53. Rannikko JH, Hollmén M. Clinical landscape of macrophage-reprogramming cancer immunotherapies. Br J Cancer. 2024;131(4):627-40. doi:10.1038/s41416-024-02715-6
54. Liu WL, Yalcinkaya M, Maestre IF, Olszewska M, Ampomah PB, Heimlich JB, et al. Blockade of IL-6 signaling alleviates atherosclerosis in Tet2-deficient clonal hematopoiesis. Nat Cardiovasc Res. 2023;2(6):572-86. doi:10.1038/s44161-023-00281-3
55. Bent EH, Millán-Barea LR, Zhuang I, Goulet DR, Fröse J, Hemann MT. Microenvironmental IL-6 inhibits anti-cancer immune responses generated by cytotoxic chemotherapy. Nat Commun. 2021;12:6218. doi:10.1038/s41467-021-26407-4
56. Lapalombella R, Yeh YY, Wang L, Ramanunni A, Rafiq S, Jha S, et al. Tetraspanin CD37 directly mediates transduction of survival and apoptotic signals. Cancer Cell. 2012;21(5):694-708.
57. Lukey MJ, Cluntun AA, Katt WP, Lin MCJ, Druso JE, Ramachandran S, et al. Liver-type glutaminase GLS2 is a druggable metabolic node in luminal-subtype breast cancer. Cell Rep. 2019;29(1):76-88.
58. Saha SK, Islam SMR, Abdullah-Al-Wadud M, Islam S, Ali F, Park KS. Multiomics analysis reveals that GLS and GLS2 differentially modulate the clinical outcomes of cancer. J Clin Med. 2019;8(3):355.
59. Dias MM, Adamoski D, dos Reis LM, Ascenção CFR, de Oliveira KRS, Mafra ACP, et al. GLS2 is protumorigenic in breast cancers. Oncogene. 2020;39:690-702.
60. Xiang L, Xie G, Liu C, Zhou J, Chen J, Yu S, et al. Knock-down of glutaminase 2 expression decreases glutathione, NADH, and sensitizes cervical cancer to ionizing radiation. Biochim Biophys Acta. 2013;1833(12):2996-3005.
61. Jin J, Byun JK, Choi YK, Park KG. Targeting glutamine metabolism as a therapeutic strategy for cancer. Exp Mol Med. 2023;55:706-15.